Journal of Medicinal and Nanomaterials Chemistry 3 (2023) 186-198

*Journal of Medicinal and Nanomaterials Chemistry*

*Journal homepage: https://jmnc.samipubco.com/*

Original Research Article

# PZT and SrCeO as catalysts, their Synthesis and Applications in Alcohol Fuel Cell

**Nabtahil Iqbal[1], Shakir Khan[2], Fawad Ahmad[1]***

[1] *Department of Chemistry, University of Wah, Quaid Avenue, Wah Cantt., Punjab, Pakistan*
[2] *Ibn -e- Sina Institute of Technology, Islamabad, Pakistan*

**ARTICLE INFORMATION**

Received: 30 June 2023
Received in revised: 16 August 2023
Accepted: 18 August 2023
Available online: 19 August 2023
Checked for Plagiarism: **YES**

DOI: 10.48309/JMNC.2023.3.2

**KEYWORDS**

Fuel cell
EOR
PZT
SrCeO
Catalysis

**ABSTRACT**

Rising energy consumption and depleting fossil fuel availability are the key issues and concerns about the impact of using traditional fossil fuels on human health. Compared to well-known Internal Combustion Engine (ICE) technologies, fuel cells (FCs) are efficient and environmentally friendly tools that electrochemically transform the chemical energy of fuels like $H_2$, natural gas, methanol, ethanol and hydrocarbons into electric energy with significantly higher efficiency and much lower greenhouse gas emission. Despite having many advantages, there is a need for developing an electrode catalyst that has comparable activity to standard Pt or other noble metal catalysts, but it should also be cost cost-effective. In this regard, lead zirconium titanate (PZT) and strontium cerium oxide (SrCeO) catalysts have been synthesized through hydrothermal technique. These materials were then characterized using a scanning electron microscope (SEM), X-ray diffraction (XRD) analysis, and thermal gravimetric analysis (TGA). The average size of the PZT from the SEM was 0.9 µm, and SrCeO was 1.82 µm. The purity and crystallinity of both materials were observed from the XRD pattern. TGA of PZT shows 26.7% weight loss up to 500 °C, while SrCeO shows 5.1% weight loss up to 650 °C. The electrochemical behavior in alcohol fuel cells is expressed through cyclic voltammetry, Linear Sweep Voltammetry, tafel plot and chronoamperometry.

Corresponding author, email: fawad.ahmad@uow.edu.pk (F. Ahmad).

**Graphical Abstract**

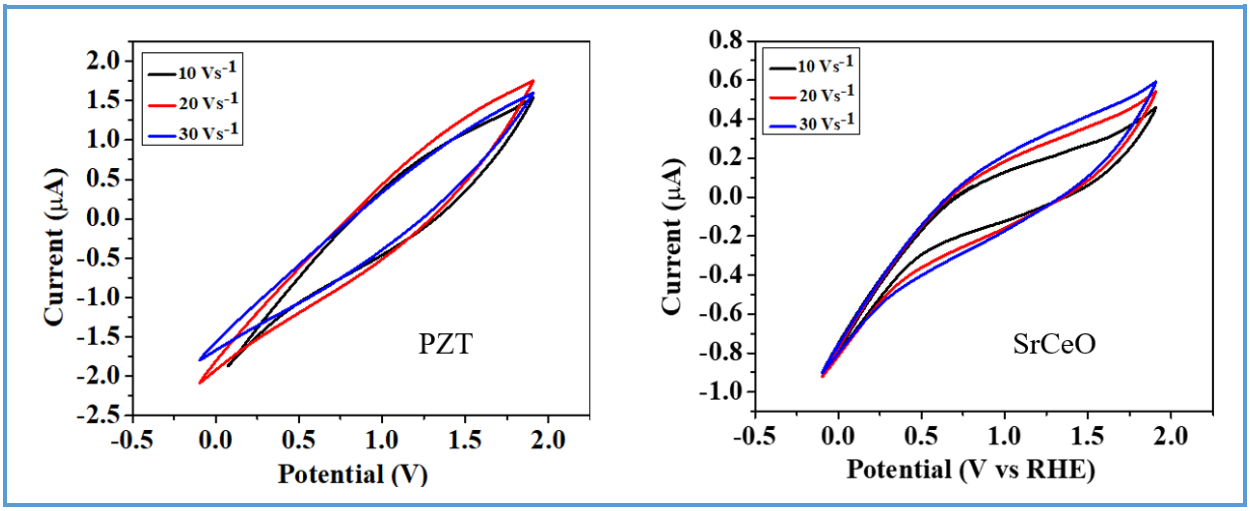


## Introduction

The availability of reliable energy sources at moderate prices has become an exception worldwide [1]. Lately, the rising pressure for energy needs is increasing the demand for energy production devices [2, 3]. Energy is the critical element for all human activities, including domestic usage, agriculture, and transportation, and is depleting the reserves of energy sources [4, 5]. A fuel cell (FC) isconsidered a “factory” that uses fuel as an input and generates electricity as an output. This factory will continue to produce electricity as long as the raw material (fuel) is provided [6].

One of the most promising new energy sources is thought to be FCs since they are environmentally benign machines that convert chemical energy from renewable sources into a theoretically highly efficient and powerful form of electrical energy. It can power vehicles as well as mobile and stationary gadgets. Compared to conventional Internal Combustion Engines (ICE), FCs are cleaner, more efficient and stable devices [7]. Moreover, compared to the ICE, it has higher efficiency since it produces less noise and heat [8].

In the initial stage of FC development, only Pt black nanoparticles were used as catalysts for the anode and cathode [9]. The sluggish kinetics of the reaction demands high loading of precious metal-containing catalysts (i.e., Pt), which unfavorably increases the cost of these electrochemical energy conversion devices. Therefore, the cost of FCs is directly linked to the price of Pt in the highly monopolized precious metal market. An increase in the demand for FC power systems is bound to drive up the already high price of Pt. At this juncture, the electrocatalysts' catalytic efficiency must be substantially improved to significantly weaken or fully eliminate the dependency on noble Pt [10]. Therefore, the current research focuses on synthesizing different catalysts to enhance FC performance. Due to the perovskite structure of Lead Zirconium Titanate (PZT), it can be a suitable catalyst. Moreover, some of the strontium compounds also show the perovskite structure. Hence, the designed catalysts can be utilized to improve FC efficiency, durability and reliability and reduce cost, allowing them to compete against traditional energy-converting devices in the market.

*Ethanol Oxidation Reaction (EOR)*

During the ethanol oxidation process that takes place in Direct Ethanol FC (DEFC), (a) an aqueous ethanol solution is fed from the anode side to the electrode surface, where it undergoes oxidation, producing $CO_2$ as well as electrons and protons; (b) protons and electrons diffuse through the membrane and external circuit, respectively; and (c) $O_2$ is reduced at the cathode surface by accepting the external electrons and the internal protons. The reaction is represented below in Equation

$$CH_3OH + 3O_2 \rightarrow 2CO_2 + 3H_2O \quad (1)$$

Complete oxidation involves $12e^-$ transfer while incomplete oxidation includes $4e^-$ transfer as shown below in Equation (2-5):

$$C_2H_5OH + 3H_2O \rightarrow 2CO_2 + 12H^+ + 12e^- \quad (2)$$

$$C_2H_5OH + 5H_2O \rightarrow 2HCO_3 + 12H^+ + 12e^- \quad (3)$$

$$C_2H_5OH + 5H_2O \rightarrow 2CO_3^{-2} + 16H^+ + 12e^- \quad (4)$$

$$O_2 + 4H^+ + 4e^- \rightarrow 2H_2O \quad (5)$$

DEFCs are electrochemical systems that transform liquid ethanol's chemical energy into electricity [11]. Ethanol is a clean, sustainable fuel naturally found in considerable quantities in biomass. Its oxidation to $CO_2$ and $H_2O$ (12 $e^-$ exchanged in the required electrocatalytic process) would result in high energy densities. Additionally, ethanol's ease of handling, storage and transportation help to avoid some of the issues that come with gaseous fuel like $H_2$ systems. Pt is the most effective pure metal catalyst for the EOR during the past few decades.

On the other hand, Pt is vulnerable to deactivation due to the adsorption of certain intermediates (such as CO) and reaction by-products throughout the various chemical paths. The need for more efficient and reliable EOR electrocatalysts has been spurred by this fact and the high price of Pt [12]. This study is based on synthesizing PZT and SrCeO as a catalyst to meet the goal.

## Chemicals and Synthesis

### *Chemicals Utilized*

The chemicals utilized for the synthesis were Lead Oxide, Zirconium Oxide, Titanium dioxide, Strontium Oxide, Cerium Oxide, Ethanol, Iso-propanol, Potassium Hydroxide and Nafion. All the chemicals were purchased from Sigma Aldrich. They were of analytical grade and were used without any further purification. A hydrothermal technique was used to synthesize both catalysts.

### *Synthesis of PZT*

$ZrO_2$ (4.508g), PbO (6.620 g) and $TiO_2$ (0.767 g) suspension were added in stoichiometric proportions to a Teflon lined autoclave with a capacity of 100 mL, which was then 80% filled with $H_2O$. Then, KOH (22.40 g) was gradually added while being stirred; the KOH concentration at this point was 5 mol/L. The autoclave was kept at 120-265 °C for 1-10 h before naturally cooling to ambient temperature. Following filtering, the products were successively washed with distilled $H_2O$ and ethanol. The product was then dried at 80 °C. The schematic representation of the synthetic technique is illustrated in Figure 1.

### *Synthesis of SrCeO*

SrO (4.508g) and CeO (6.620g) were added in stoichiometric proportions to a Teflon-lined autoclave with a 100 mL capacity of 80% filled with $H_2O$. Then, KOH (22.40 g) was gradually added while being stirred; the KOH concentration at this point was 5 mol/L. The autoclave was kept at 120-265 °C for 1-10 h before naturally cooling to ambient temperature. Following filtering, the product was successively washed with distilled $H_2O$ and ethanol. It was then dried at 80 °C. The schematic representation of the synthetic method is shown in Figure 2.

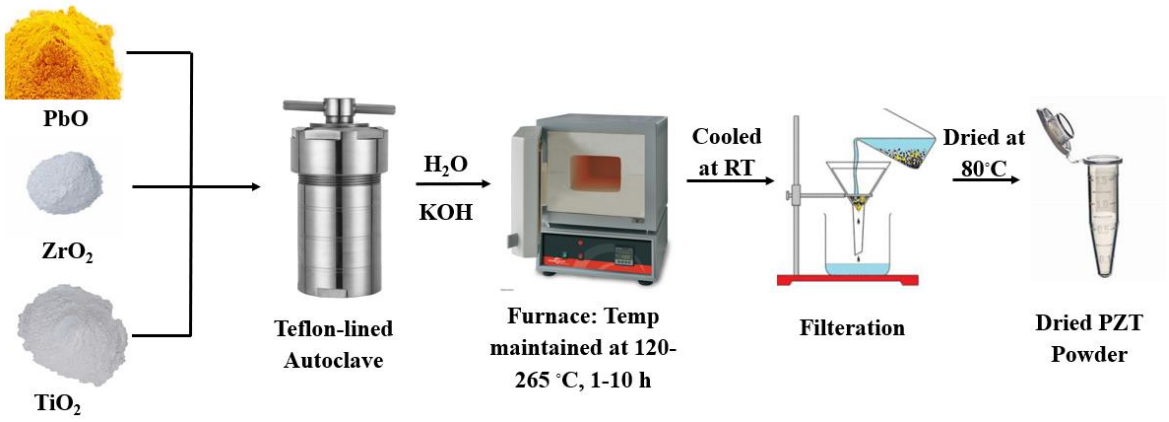


**Figure 1.** Schematic diagram of the preparation of PZT

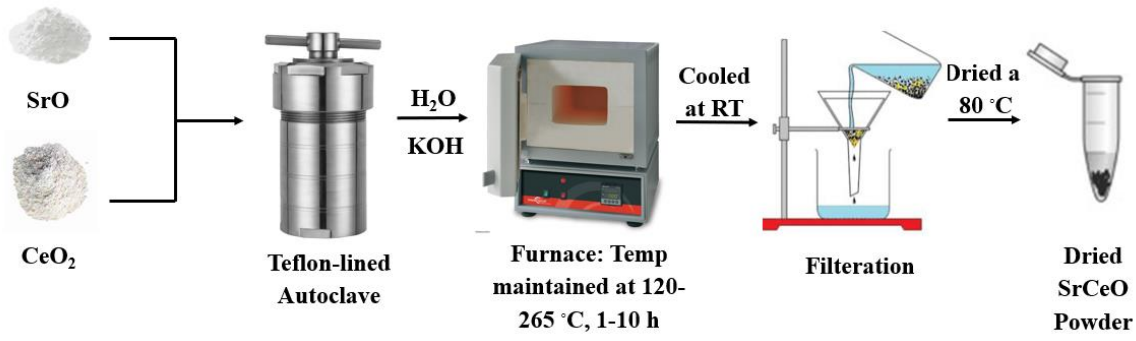


**Figure 2.** Schematic diagram of the preparation of SrCeO

## Characterization Techniques

*SEM*

The synthesized catalysts' surface texture and grain size were assessed using high-resolution SEM analysis. The granules are randomly dispersed, as shown in Figure 3 (a, b) and Figure 5 (a, b). It is observed that the particles do not have a definite shape. They appeared to be flaky stones/ rocks and were in an agglomeration state. Agglomeration may develop as a result of the particles' magnetic interactions.

Moreover, the surface of the particles was not homogenous because of the polydisperse system (non-uniformity in size distribution) [13]. The maximum and minimum particle sizes calculated through nano measurer are 2.93 µm and 0.25 µm under a 1 µm scanning lens for PZT. The average particle size present is 0.91 µm (Figures 3a and 4a). The maximum and minimum particle sizes calculated through nano measurer are 4.27 µm and 0.77 µm under a 5 µm scanning lens. The average number of particle size present is 1.82 µm (Figures 3b and 4b) for PZT.

The maximum and minimum particle sizes calculated are 2.86 µm and 0.27 µm under a 1 µm scanning lens. The average particle size present is 0.96 µm (Figures 5a and 6a) for SrCeO. The maximum and minimum particle sizes are 1.86 µm and 0.12 µm under a 1µm scanning lens. The average particle size present is 0.56 µm (Figures 5b and 6b) for SrCeO. [14].

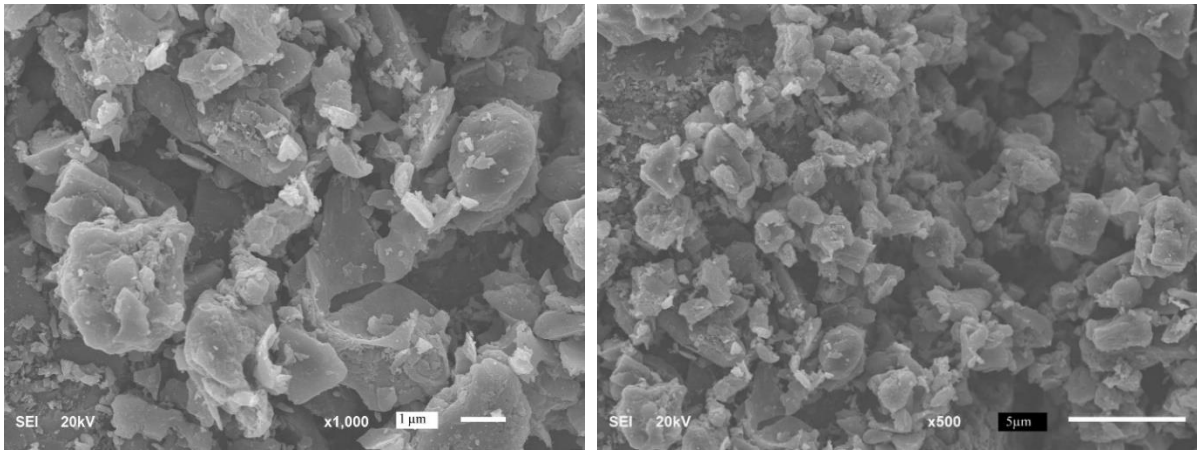


(a) (b)

**Figure 3.** SEM images of PZT at bar scale (a) 1 µm and (b) 5 µm

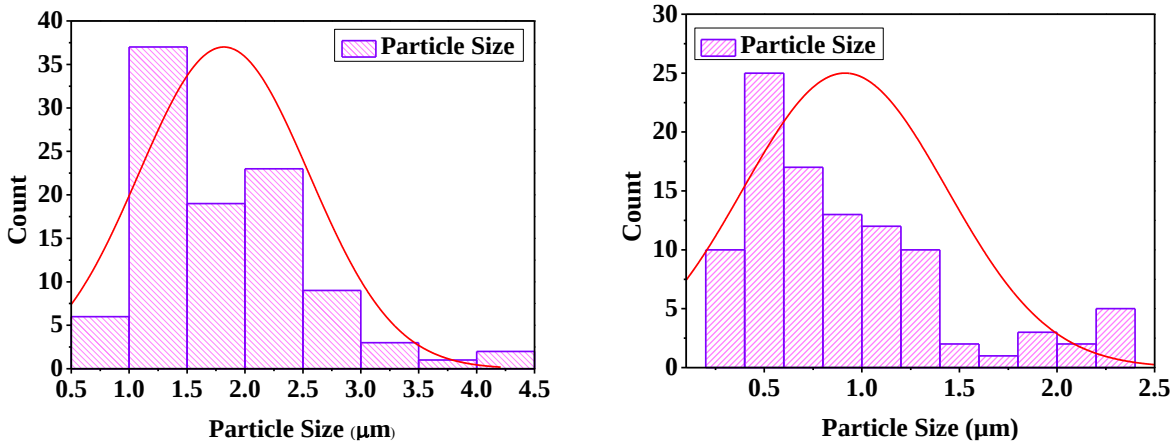


**Figure 4.** Distribution curves of corresponding SEM images (a=1µm, b=5µm)

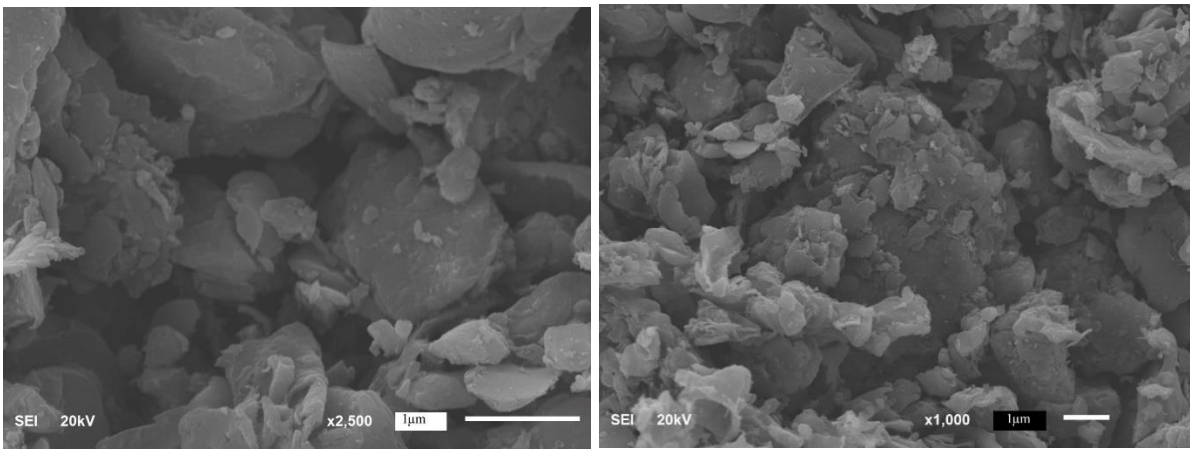


**Figure 5.** SEM images of SrCeO at bar scale 1 µm

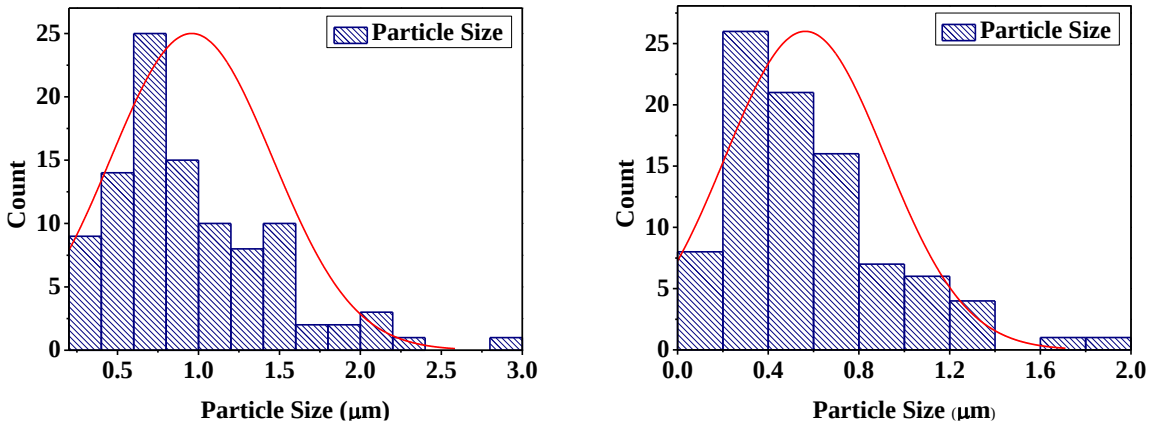


**Figure 6.** Distribution curves of corresponding SEM images

*XRD*

The synthesized materials were subjected to a crystallographic analysis using the XRD technique. The absence of specular diffractions denotes crystallographic purity. No contaminant peaks were detected, confirming the purity of the synthesized compounds. The XRD peaks indicated the formation of PZT (100), (110), (111), (200), (211), (022), at 22.1, 31.08, 38.06, 44.46, 54.98, and 65 stated in literature [15] and depicted in Figure 7a while SrCeO (110), (200), (220), (311), (222), (331), (420), (422) at 28.1, 33.5, 47.46, 57.59, 60.04, 70.02, 77.34 and 79.43 described in the literature (JCPDS no: 34-0394) [16], as seen in Figure 7b. The data determined the crystallite size to be 4.69 nm and 28.69 nm for PZT and SrCeO, respectively. The strong diffraction peaks demonstrate the samples' outstanding crystallinity.

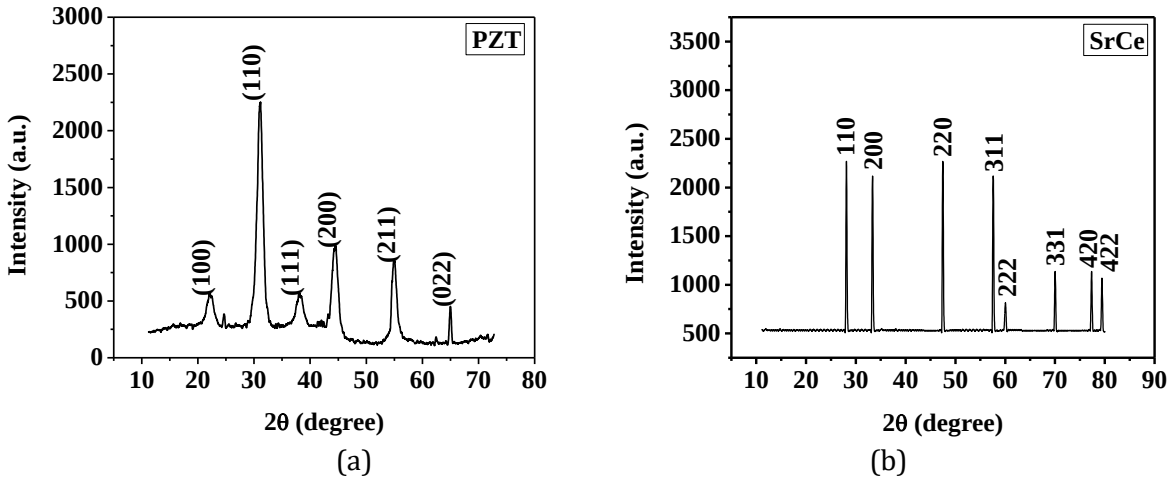


**Figure 7.** XRD patterns of (a) PZT and (b) SrCeO (JCPDS no: 34-0394)

*TGA/DTA*

The findings of the differential analysis (DTA) and thermogravimetric analysis (TGA)

for PZT are displayed in Figure 8a. The TG curve declines until it reaches a horizontal at about 600 °C. The horizontal curve relates to PZT's existence. Three significant regions may be seen on the TGA and DTA traces. The water loss occurs from the temperature range of about 215-300 °C, followed by an endothermic reaction, a small amount of decomposition, and a weight loss of 3% and 15.7%, respectively. Finally, the development of the PZT perovskite structure and 8% weight loss are related to the third deflection, which happened at about 400 °C. The total weight loss from 0-600 °C is estimated to be 26.7%, after which no further weight loss is observed following the literature [17]. The TGA/DTA horizontal curves are reached at about 600 °C, indicating that the perovskite PZT has completed its formation at a furnace temperature over 600 °C.

The TGA/DTA curves for SrCeO (Figure 8b) show a three-stage weight loss trend. Since the intermediate resins are not entirely dried and can readily absorb $H_2O$, the first stage of the TGA profile with a span of 75 °C is attributed to the loss of $H_2O$ with an average weight loss of 0.6%. The disintegration of the associated coordination species, which corresponds to the exothermic peaks at 150 or 300 °C in DTA curves, causes the second stage, a rapid weight loss stage, which is reported to occur at a temperature range of 140 °C and claims around 2.2%. The third stage is 2.3% weight loss, which is more pronounced between 530 and 630 °C [18].

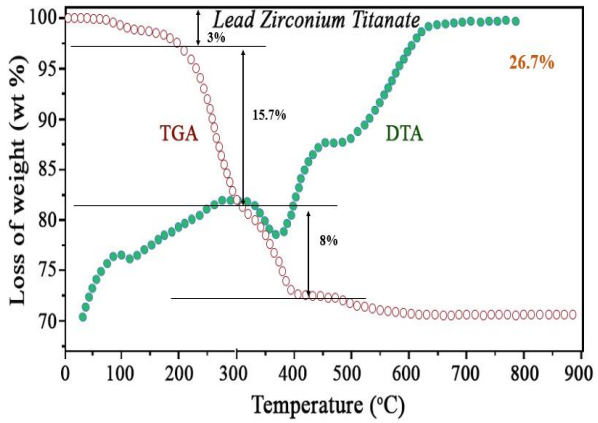


(a)

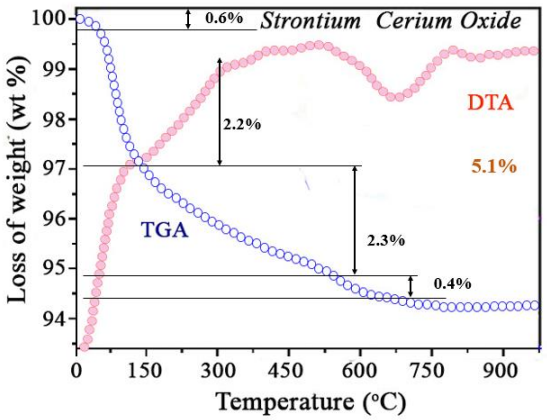


(b)

**Figure 8.** TGA/DTA for (a) PZT and (b) SrCeO

## Results and Discussion

*Electrochemical Analysis*

The electrochemical analysis was done using Potentiostat. Cyclic Voltammetry (CV) was performed to determine the catalyst's Mass activity and Electrochemically Active Surface Area (ECSA). Linear Sweep Voltammetry (LSV) was utilized to study the factors like over potential, onset potential and Tafel plot of the catalyst, while Chronoamperometry (CA) was used to study the catalysts' stability.

*Mass Activity*

CV for PZT and SrCeO (Figures 9a and b) was used to study the mass activity of the catalysts. As we increase the scan rate, the current response increases due to the enhancement in the diffusion rate. This increase in current causes a rise in the mass activity of the catalyst.

The results shown in Table 1 follow the trend explained. The mass activity values calculated from CV (Figure 9a and b ) for our prepared catalysts (PZT= 1.7 mA or 1759.3 μAmg$^{-1}$ ) and SrCeO (5.8 mAmg-1 584.1 μAmg$^{-1}$) are somewhat lower as compared to the commercially available catalysts such as Pt/C at= 4 mAmg$^{-1}$ and Pd/C= 25.4 mAmg$^{-1}$.

LSV plots (Figure 10a and b) were used to study parameters like overpotential, the onset potential and tafel slope values for both catalysts.

*Over Potential*

Overpotential indicates extra potential required concerning equilibrium potential to facilitate a redox reaction. The presence of overpotential in an electrolytic cell indicates that the cell needs more energy than what is predicted by thermodynamics to drive a reaction. It happens due to the high activation energy required for electron transport at the electrodes and is crucial for releasing gases like $H_2$ and $O_2$. The catalyst with low over-potential losses is better [20]. The one with high over-potential losses represents decreased activity [21].

The overpotential for PZT (1.6771 V or 1677.7 mV) and SrCeO (1.6782 V or 1678.2 mV) in comparison to Pt/C= 2.13 mV and Pd= 1.67 mV is shown in Table 2.

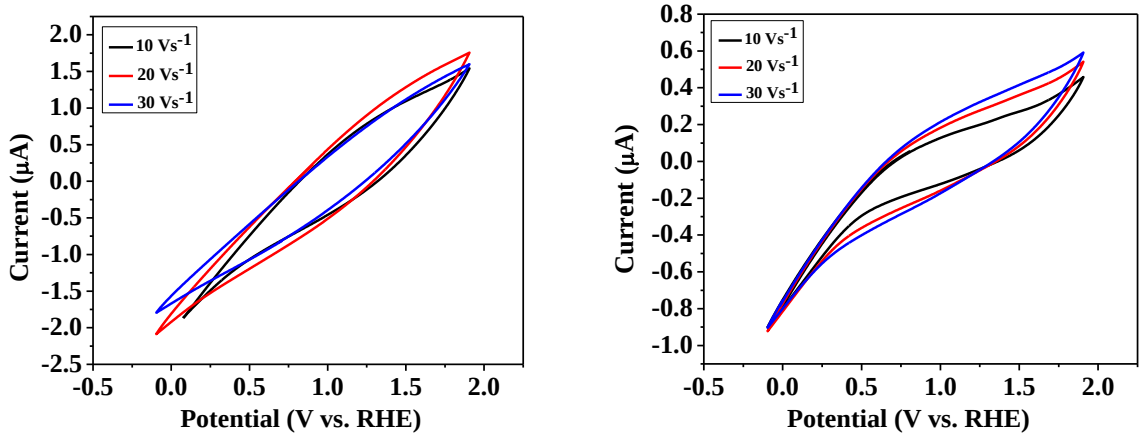


**Figure 9.** CV curves of (a) PZT and (b) SrCeO

**Table 1**. Mass Activity of PZT and SrCeO

| Activity | Scan Rate (Vs$^{-1}$) | Standard Metal (mAmg$^{-1}$) | SrCeO (μAmg$^{-1}$) | PZT (μAmg$^{-1}$) |
|---|---|---|---|---|
| **Mass Activity** | 10 | Pt/C = 4<br>Pd/C = 25.4 [19] | 454.6 | 1524.9 |
| | 20 | | 544.1 | 1759.3 |
| | 30 | | 584.1 | 1594.8 |

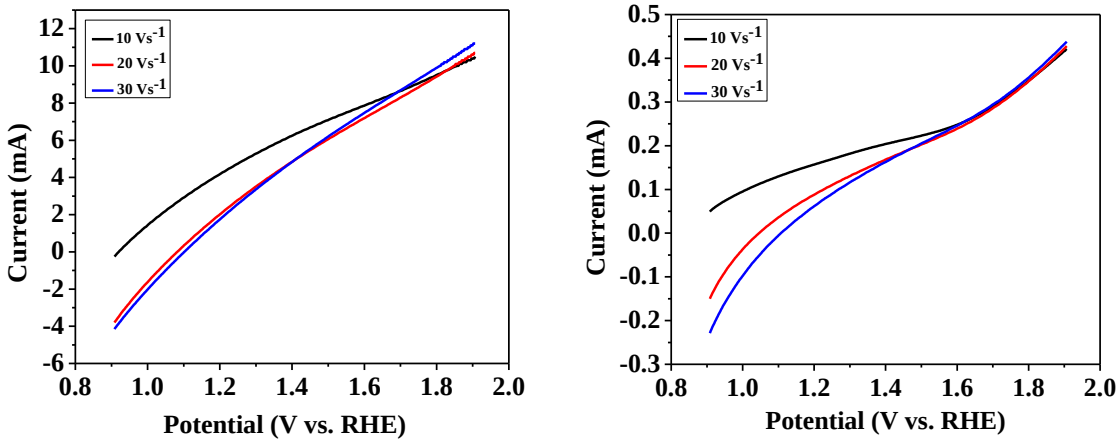


**Figure 10.** LSV of (a) PZT and (b) SrCeO

**Table 2.** Over Potential values of PZT and SrCeO

| Activity | Scan Rate ($Vs^{-1}$) | Standard Metal (mV) | SrCeO (V) | PZT (V) |
|---|---|---|---|---|
| **Over Potential** | 10 | Pt/C = 2.13 [22] Pd = 1.67 [23] | 1.6806 | 1.6782 |
| | 20 | | 1.6782 | 1.6771 |
| | 30 | | 1.6817 | 1.6771 |

*Onset Potential*

Onset potential can be determined by drawing two tangents, one from the baseline (non-faradic region) and the other from the rising current (faradic region). The point where they join is said to be the onset potential [24]. A low value of onset potential is an indication of efficient metal for EOR.

The onset potential value in our catalysts is comparable to Pt/C (1.36 V) and Pd (0.9 V), which shows better activity of the catalysts. Onset potentials for PZT (0.9071 V) and SrCeO (0.9082 V) are listed in Table 3.

*Current Density*

As already discussed, the current response increases with the increase in scan rate due to the rise in the diffusion rate, which can be seen in Table 4. However, our catalysts have shown a lower amount of current response when compared with the standard catalysts (Table 4). The current density for PZT is 2.4548 $\mu Acm^{-2}$, while that for SrCeO is 0.8205 $\mu Acm^{-2}$. Whereas, Pd/C shows 27 $mAcm^{-2}$ current density.

*Tafel Slope*

Replotting the polarization curves, i.e., LSV as log current density (j or i) versus overpotential, yields the tafel plot [26].

$$\boldsymbol{\eta = a + b}\,log\,\mathbf{j} \qquad (6)$$

Where "$\boldsymbol{\eta}$"is overpotential, "a" is the tafel constant, "b" is the tafel slope and "j" refers to current density. As we can see in Equation 6, "a" takes on the unit of potential when log(j) equals

zero. Additionally, if j is given in the unit of $mAcm^{-2}$, a assumes the overpotential value at 1 $mAcm^{-2}$. If the onset potential is defined as the potential needed to reach 1 $mAcm^{-2}$, then the tafel constant directly denotes the onset potential. Tafel constant can be realized as the onset potential because $mAcm^{-2}$ is frequently employed in the literature as the unit of current density. This reasoning implies that the lower the value of an (onset potential), the lower the Tafel slope value, and hence better will be the catalyst [27]. Figure 11 (a and b) reveals the tafel plots for PZT and SrCeO, respectively.

The Tafel slope value for PZT is -7.0272±0.57034 $Vdec^{-1,}$ and that for SrCeO is -7.3709±0.49159 $Vdec^{-1}$, while our standard Pt has a tafel value of 170±10 $Vdec^{-1}$ as shown in Table 5.

**Table 3.** Onset Potential values of PZT and SrCeO

| Activity | Scan Rate ($Vs^{-1}$) | Standard Metal (V) | SrCeO (V) | PZT (V) |
|---|---|---|---|---|
| **Onset Potential** | 10 | Pt/C = 1.36 [22] Pd = 0.9 [23] | 0.9106 | 0.9082 |
| | 20 | | 0.9082 | 0.9071 |
| | 30 | | 0.9117 | 0.9071 |

**Table 4.** Current Density values of PZT and SrCeO

| Activity | Scan Rate ($Vs^{-1}$) | Standard Metal ($mAmg^{-1}$) | SrCeO ($\mu Acm^{-2}$) | PZT ($\mu Acm^{-2}$) |
|---|---|---|---|---|
| **Current Density** | 10 | Pt/Vulcan= 0.5 | 0.6345 | 2.1179 |
| | 20 | Pd/G= 0.8 | 0.7433 | 2.4548 |
| | 30 | Pd/C (commercial) = 27 [25] | 0.8205 | 2.2005 |

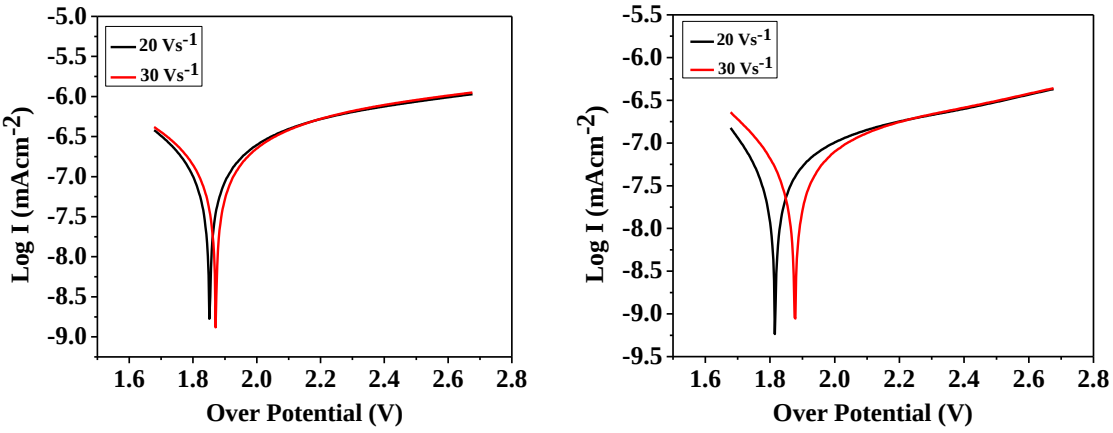


**Figure 11.** Tafel slope of (a) PZT and (b) SrCeO

*Chronoamperometry*

PZT and SrCeO CA curves are depicted in Figure 12 (a and b), respectively. Chronoamperometry experiments were carried out to estimate the steady-state activity of the catalysts for the EOR at about 500 s. It was observed that the current density declined for a short period of about 100 s, but then it became constant for 500 seconds, predicting improved stability for both PZT and SrCeO.

**Table 5.** Tafel Slope values of PZT and SrCeO

| Activity | Scan Rate ($Vs^{-1}$) | Standard Metal ($Vdec^{-1}$) | SrCeO ($Vdec^{-1}$) | PZT ($Vdec^{-1}$) |
|---|---|---|---|---|
| **Tafel Slope** | 20 | Pt/C= 170±10 | -7.5248±0.64271 | -7.0600±0.59991 |
| | 30 | [19] | -7.3709±0.49159 | -7.0272±0.57034 |

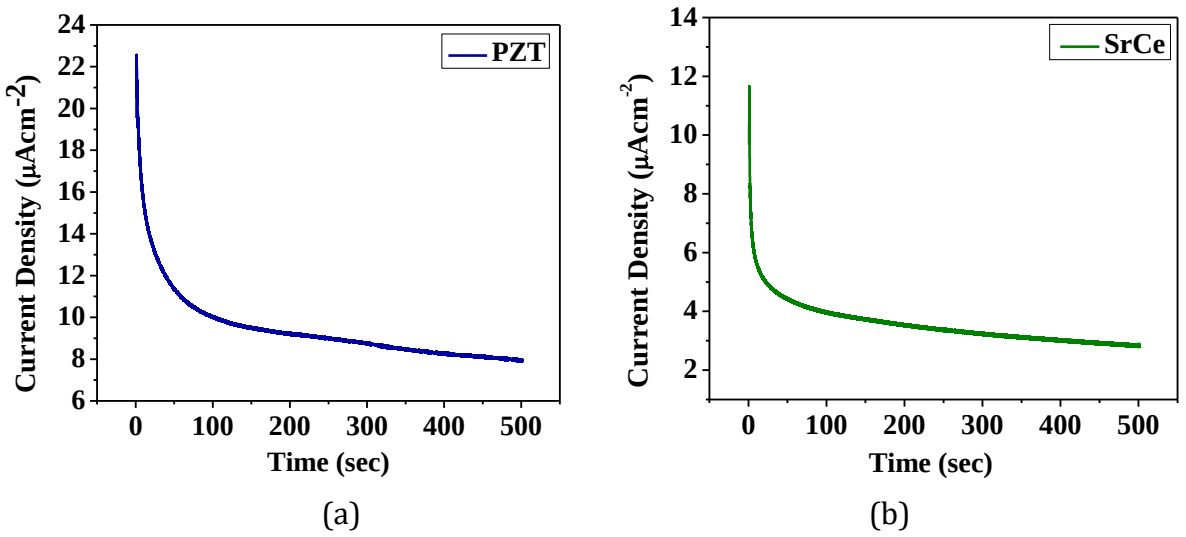


(a) (b)

**Figure 12.** Chronoamperometry curve of (a) PZT and (b) SrCeO at 500 seconds

## Conclusion

Two efficient fuel cell catalysts, i.e., Lead Zirconium Titanate (PZT) and Strontium Cerium Oxide (SrCeO), were prepared. A hydrothermal technique was used to synthesize the catalysts. The crystallite size was recorded as 4.696124 nm (PZT) and 28.69723 nm (SrCeO) through powder XRD. The catalysts had a flaky stone kind of morphology, which SEM confirmed. TGA/DTA had proven the high thermal stability of both catalysts at a high temperature of about 800 °C.

Regarding application, both catalysts were checked for EOR reaction in a fuel cell. A higher value of overpotential, SrCeO (525 mV), and PZT (516.8 mV) were recorded in comparison to the Pt standard (300 mV) for ORR and SrCeO (1678.2 mV), PZT (1677.7 mV) in comparison to Pd (1.67 mV) for EOR. EOR activity for both the catalysts was good in terms of lower cost and lower value of onset potential, but mass activity and tafel values were higher than the standard, which shows that our material can be utilized as a fuel cell catalyst as it gives the advantages of lower cost and less potential losses.

**Acknowledgment**

This work is financially supported by the Chemistry Department, University of Wah.

**Disclosure Statement**

No potential conflict of interest was reported by the authors.

**Orcid**

*Nabtahil Iqbal*: 0009-0002-9357-6289
*Fawad Ahmad*: 0000-0003-2404-5572
*Shakir Khan*: 0009-0001-9735-0140

**References**

[1]. Kebede A.A., Kalogiannis T. ,Mierlo J.V., Berecibar M. *Renew. Sustain. Energy Rev.*, 2022, **159**:112213 [CrossRef], [Google Scholar], [Publisher]
[2]. Abdalla A.N., Nazir M.S., Tao H., Cao S., Ji R., Jiang M., Yao L. *J. Energy Storage*., 2021, **40**:102811 [CrossRef], [Google Scholar], [Publisher]
[3]. Hargreaves T., Middlemiss L. *Nat. Energy*, 2020, **5**:195 [CrossRef], [Google Scholar], [Publisher]
[4]. Moussa R.R., Mahmoud A.H., Hatem T.M. *J. Clean. Prod.*, 2020, **254**:119932 [CrossRef], [Google Scholar], [Publisher]
[5]. Moussa R.R., Mahmoud A.H. *J. Clean. Prod.*, 2017, **153**:114 [CrossRef], [Google Scholar], [Publisher]
[6]. O'hayre R., Cha S.W., Colella W., Prinz F.B. *Fuel Cell Fundamentals*; Wiley Online Library, 2016. [Google Scholar]
[7]. Ren X., Wang Y., Liu A., Zhang Z., Lv Q., Liu B. *J. Mater. Chem. A.*, 2020, **8**:24284 [CrossRef], [Google Scholar], [Publisher]
[8]. Esfe M.H., Afrand M. *J. Therm. Anal. Calorim.*, 2020, **140**:1633 [CrossRef], [Google Scholar], [Publisher]
[9]. Huang L., Zaman S., Tian X., Wang Z., Fang W., Xia B.Y. *Acc. Chem. Res.*, 2021, **54**: 311 [CrossRef], [Google Scholar], [Publisher]
[10]. Zhang W., Chang J., Yang Y. *Sus. Mat.*, 2023, **3**:2 [CrossRef], [Google Scholar], [Publisher]
[11]. Liang Z.X., Zhao T.S., Xu J.B., Zhu L.D. *Electrochim. Acta.*, 2009, **54**:2203 [CrossRef], [Google Scholar], [Publisher]
[12] Rizo R., Arán-Ais R., Padgett E., Muller D., Lázaro M.J., Solla-Gullon J., Feliu J.M., Pastor E., Abruña H.D. *J. Am. Chem. Soc.*, 2018, **140**:3791 [CrossRef], [Google Scholar], [Publisher]
[13]. ul Ain Q., Fazal S., Ahmad F. *J. Chem. Environ.*, 2023, **2**:1 [CrossRef], [Google Scholar], [Publisher]
[14]. Fazal S., Ahmad F., Shah K.H., Shahida S., Ahmad T., Nasar G. *J. Mater. Phys. Sci.*, 2023, **4**:1 [CrossRef], [Google Scholar], [Publisher]
[15]. Oliveiran C.A., Longo E., Varela J.A., Zaghete M.A. *Ceram. Int.*, 2014, **40**:1717 [CrossRef], [Google Scholar], [Publisher]
[16]. Zhou L., Li X., Yao Z., Chen Z., Hong M., Zhu R., Liang Y., Zhao J. *Sci. Rep.*, 2016, **6**:23900 [CrossRef], [Google Scholar], [Publisher]
[17]. Zak A.K., Majid W.H.A. *Ceram. Int.*, 2010, **36**:1905 [CrossRef], [Google Scholar], [Publisher]
[18]. Kumar E., Selvarajan P., Balasubramanian K. *Recent Res. Sci. Technol*, 2010, **2**:37 [Google Scholar]
[19]. Delpeuch A.B., Asset T., Chatenet M., Cremers C. *Fuel Cells.*, 2015, **15**:352 [CrossRef], [Google Scholar], [Publisher]
[20]. Sun S., Li H., Xu Z.J. *Joule*, 2018, **2**:1024 [CrossRef], [Google Scholar], [Publisher]
[21]. Yaqoob L., Noor T., Iqbal N. *RSC Adv.*, 2021, **11**:16768 [CrossRef], [Google Scholar], [Publisher]

[22]. Ma K.B., Han D.H., Park S.B., Kim H.S., Won D.H., Won J.E., Kwon S.H., Kim M.C., Moon S.H., Park K.W. *ACS Sustainable Chem. Eng.*, 2018, **6**:7609 [CrossRef], [Google Scholar], [Publisher]
[23]. Zhang R.L., Duan J.J., Han Z., Feng J.J., Huang H., Zhang Q.L., Wang A.J. *Appl. Surf. Sci.*, 2020, **506**:144791 [CrossRef], [Google Scholar], [Publisher]
[24]. Huang Z.F., Wang J., Peng Y., Jung C.Y., Fisher A., Wang X. *Adv. Energy Mater.*, 2017, **7**:1700544 [CrossRef], [Google Scholar], [Publisher]
[25]. Kazan E.S., Bayramoğlu M. *Int. J. Energy Res.*, 2021, **45**:12806 [CrossRef], [Google Scholar], [Publisher]
[26]. Raveendran A., Chandran M., Dhanusuraman R. *RSC Adv.*, 2023, **13**:3843 [CrossRef], [Google Scholar], [Publisher]
[27]. Murthy A.P., Theerthagiri J., Madhavan J. *J. Phys. Chem. C*, 2018, **122**:23943 [CrossRef], [Google Scholar], [Publisher]

How to cite this manuscript: Nabtahil Iqbal, Shakir Khan, Fawad Ahmad*. PZT and SrCeO as catalysts, their Synthesis and Applications in Alcohol Fuel Cell. *Journal of Medicinal and Nanomaterials Chemistry*, 2023, 5(3), 186-198. DOI: 10.48309/JMNC.2023.3.2